International Journal of Thermophysics, Vol. 27, No. 2, March 2006 (© 2006)
DOI: 10.1007/s10765-005-0003-4

Thermal Conductivity of Small Nickel Particles

S. P. Yuan[1] **and P. X. Jiang**[1,2]

Received October 26, 2004

The thermal conductivity of nanoscale nickel particles due to phonon heat transfer is extrapolated from thin film results calculated using nonequilibrium molecular dynamics (NEMD). The electronic contribution to the thermal conductivity is deduced from the electrical conductivity using the Wiedemann–Franz law. Based on the relaxation time approximation, the electrical conductivity is calculated with the Kubo linear-response formalism. At the average temperature of $T = 300\,\mathrm{K}$, which is lower than the Debye temperature $\Theta_D = 450\,\mathrm{K}$, the results show that in a particle size range of 1.408–10.56 nm, the calculated thermal conductivity decreases almost linearly with decreasing particle size, exhibiting a remarkable reduction compared with the bulk value. The phonon mean free path is estimated, and the size effect on the thermal conductivity is attributed to the reduction of the phonon mean free path according to the kinetic theory.

KEY WORDS: nanoscale; nickel particles; nonequilibrium molecular dynamics (NEMD); thermal conductivity.

1. INTRODUCTION

The thermodynamic properties of nanoparticles play an important role in understanding the transition from the microscopic structure to macroscopic structure of matter. Nickel nanoparticles have potential importance in the physics and chemistry of transition metals [1]. Nickel particles are of special interest because of their practical applications in catalysts, nanoporous media, ferromagnetism, and their superparamagnetic behavior [2–4].

[1] Key Laboratory for Thermal Science and Power Engineering, Department of Thermal Engineering, Tsinghua University, 100084 Beijing, P. R. China.
[2] To whom correspondence should be addressed. E-mail: Jiangpx@mail.tsinghua.edu.cn

Compared with the bulk material, nanoparticles usually contain more voids and lower packing density, more defects and impurities and, in most cases, boundary roughness and smaller grain sizes. While each of these factors could reduce the thermal conductivity, their relative importance differs. More voids and a lower packing density would lower the thermal conductivity. However, calculations show that such changes only produce a modest change in the thermal conductivity and are unlikely to explain the observed drastic reduction [5]. Hence other factors, namely the finite particle size, the boundary condition and the reduced grain size as well as the defects and impurities, should be analyzed carefully to understand the microscopic origin of the heat conduction mechanisms.

Thermal transport in metals is a function of the phonon heat transport and the electron heat transport. In pure bulk metals, the phonon heat transfer will be completely swamped by the much larger electron heat transfer [6]. But in nanoscale metallic materials, the electronic contribution to the thermal conductance decreases dramatically [7] and the thermal conductivity also decreases [8] due to the phonon heat transfer.

Numerical simulations can be used to predict the thermophysical properties of materials at nanoscales that cannot be experimentally measured. Molecular dynamics (MD) is a valuable tool for studying the atomic-scale properties of solids [9,10]. Classical MD methods simulate only the interaction between atomic nuclei, which means that the heat transfer due to the phonon-phonon interactions is taken into account. The success of MD simulation depends upon the accuracy of the inter-particle potential model used in the simulation. This is not a problem for insulators or semiconductors in which the electronic heat transfer is negligible. Over the last two decades, several types of potential models, such as tight-binding theory [11], pseudo-potential [12], empirical potential function [13], and embedded-atom method (EAM) [14] have been developed to describe the inter-atomic interaction of metals. In transition and noble metal systems, the EAM model, originally proposed by Daw and Baskes in 1984 [14], has been widely used to describe the energetics of metallic systems. Four different versions of the EAM model proposed by Johnson [15], Mei et al. [16], Cai and Ye [17], and Pohlong and Ram [18] have since been developed to employ different embedded functions, electron density functions, and two-body interaction functions. Among them, the versions of Johnson, Mei et al., and Cai and Ye show better agreement with the data obtained from the experiments for the isobar heat capacity of Cu, Ni, and Ag [19, 20]. Therefore, the version of Cai and Ye was selected for computing the thermal conductivity due to phonon–phonon interactions of nickel in the present study. The formulae and parameters of the EAM version are the same as those presented in the paper of Cai and Ye [17].

Thermal conductivity measurements are more difficult and inherently less accurate than electrical resistivity measurements. Therefore, the Wiedemann–Franz law is often used to convert electrical conductivity values into estimates of the thermal conductivity [6]. However, when the metallic particle size is less than 100 nm, the fine particle electrical conductivity is also extremely difficult to measure. Therefore, at nanoscale sizes, theoretical methods are used to estimate the electrical resistivity of thin metallic films and small metallic particles [21–24].

This work analyzes the electrical conductivity of nanoparticles using the Kubo linear-response formalism, with the Wiedemann–Franz law used to relate these values to the electronic component of the particle thermal conductivity. The lattice contribution to the thermal conductivity estimated using the NEMD method and theoretical analysis is added to the electronic component to obtain the total thermal conductivity of the materials.

2. ELECTRICAL CONDUCTIVITY

An expression for the electrical conductivity within the Kubo linear-response formalism was first obtained by specifically including the discrete nature of the states in the system, as well as some coupling to a dissipative mechanism. In the independent-electron approximation, the Hamiltonian for an electron in the presence of a semiclassical electromagnetic field characterized by the vector potential $\boldsymbol{A}(\boldsymbol{r}, t)$ is [23]

$$H = \left[\frac{\hat{p}^2}{2m^*} + V(\boldsymbol{r})\right] + \left[\frac{e}{2m^*c}(\hat{p}\cdot\boldsymbol{A} + \boldsymbol{A}\cdot\hat{p})\right] \equiv [H_0] + [H_1], \tag{1}$$

where we treat $H_0 = \hat{p}^2/2m^* + V(\boldsymbol{r})$ as the unperturbed Hamiltonian which satisfies $H_0|i> = \varepsilon_i|i>$ and evaluate the effects of the perturbation $H_1 = e(\hat{p}\cdot\boldsymbol{A} + \boldsymbol{A}\cdot\hat{p})/2m^*c$ to the lowest order.

Within linear-response theory, the density matrix can be approximated by

$$\hat{\rho} \approx \hat{\rho}^{(0)} + \hat{\rho}^{(1)} \tag{2}$$

where $\hat{\rho}^{(0)}$ is the density matrix of the system described by H_0 and the quasiequilibrium $\hat{\rho}^{(1)}$ is linear in the perturbation due to H_1. In addition, assuming that the electrons are coupled to some source of dissipation, e.g., electron–electron interactions, electron–phonon interactions, magnetic scattering, etc., we introduce an overall relaxation time τ ($\gamma = 1/\tau$ is the corresponding relaxation rate). The equation of motion for the density matrix of the electrons is

$$\frac{\partial \hat{\rho}(t)}{\partial t} + i[\hat{H}(t), \hat{\rho}(t)] = -\gamma[\hat{\rho}(t) - \hat{\rho}_{\mathrm{qe}}(t)], \tag{3}$$

Here, $\hat{\rho}_{\mathrm{qe}}$ is the quasi-equilibrium density matrix given by $(\exp\{\beta[\hat{H}_0 + \hat{H}_1(t) - \mu_0]\} + 1)^{-1}$ and μ_0 is the chemical potential. According to the linear-response theory, expanding the quasi-equilibrium density matrix to the lowest order, we have

$$\langle i|\hat{\rho}_{\mathrm{qe}}|j\rangle = f_i \delta_{ij} - \frac{f_i - f_j}{\varepsilon_{ij}} \langle i|\hat{H}_1|j\rangle, \tag{4}$$

where $\varepsilon_{ij} = \varepsilon_i - \varepsilon_j$, $\hat{\rho}^{(0)}|i\rangle = f_i|i\rangle$, and $f_i = \{\exp[\beta(\varepsilon_i - \mu_0)] + 1\}^{-1}$ is the Fermi–Dirac occupation factor for that state. From Eq. (3), the off-diagonal components of the density matrix are of the form,

$$\langle i|\hat{\rho}^{(1)}|j\rangle = \frac{f_i - f_j}{\varepsilon_{ij}} \frac{\varepsilon_{ij} - i\gamma}{\varepsilon_{ij} - \omega - i\gamma} \langle i|\hat{H}_1|j\rangle, \tag{5}$$

where $|i\rangle$ and $|j\rangle$ are eigenstates of H_0.

The induced current $\boldsymbol{j}_{\mathrm{ind}}$ is obtained by $Tr\{\hat{\rho}\hat{\boldsymbol{j}}\}$. In general, the induced current is composed of two parts, one is a diamagnetic contribution arising from the change in the current operator due to the vector potential, and the other is a paramagnetic term from the off-diagonal element in the density matrix. The electrical conductivity is calculated from $\boldsymbol{j}_{\mathrm{ind}} = \sigma(\omega)\boldsymbol{E}(\omega) = \sigma(\omega)(i\omega/c)\boldsymbol{A}(\omega)$. Thus,

$$\sigma(\omega) = \frac{ie^2}{m^*\omega}\left[\frac{N}{\Omega} + \frac{1}{\Omega m^*}\sum_{i\neq j}\frac{f_i - f_j}{\varepsilon_{ij}}\frac{\varepsilon_{ij} - i\gamma}{\varepsilon_{ij} - \omega - i\gamma} \times |\langle i|\hat{p}_E|j\rangle|^2\right], \tag{6}$$

where $\langle i|\hat{p}_{\mathrm{E}}|j\rangle$ is the matrix element of the momentum operator along the applied field.

The particle geometry used to calculate the electrical conductivity is shown in Fig. 1. Assuming a jellium model for the ions in the cube, we select particle-in-a-box wave functions as reasonable states;

$$\Psi_i = \left(\frac{8}{a^3}\right)^{1/2} \sin\frac{l\pi x}{a} \sin\frac{m\pi y}{a} \sin\frac{n\pi z}{a}, \quad \{l, m, n\} = 1, 2, 3, \ldots \tag{7}$$

$$\varepsilon_i = \frac{\hbar^2\pi^2}{2m^*}\left[\frac{l^2 + m^2 + n^2}{a^2}\right] \tag{8}$$

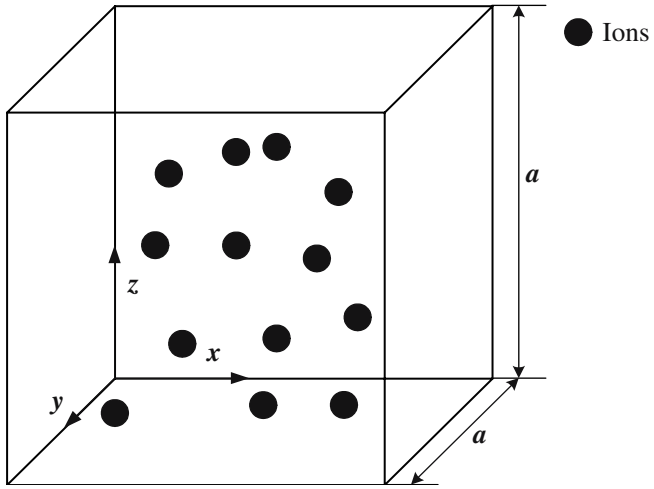

Fig. 1. Physical model for metallic particles.

Although the states for a three-dimensional highly spherical particle may be explicitly expressed in terms of spherical Bessel functions, in general, it is very cumbersome to work with their matrix elements. These would obviously be more appropriate to the experimentally occurring collections of small roughly spherical particles; the energy and general behavior of a cube and a sphere differ only in the order 1 because of the similar geometry [23].

The real part of the electrical conductivity in Eq. (6) now becomes

$$\mathrm{Re}\sigma_{\mu\mu}(\omega) = \frac{e^2}{(m^*)^2\Omega} \sum_{i\neq j} \frac{f_i - f_j}{\varepsilon_{ji}} \frac{\gamma}{(\varepsilon_{ij}-\omega)^2+\gamma^2} \times |\langle i|\hat{p}_\mu|j\rangle|^2, \tag{9}$$

The diamagnetic term in this case is exactly canceled by part of the paramagnetic term. This can be shown by invoking the well-known Thomas–Reiche–Kuhn sum rule [25] which states that independent of the choice of i,

$$\frac{2}{m^*} \sum_j \frac{|p_{ij}|^2}{\varepsilon_{ij}} = -1, \tag{10}$$

where i and j denote all the quantum numbers of a system and the matrix elements are summed over all states j. The matrix elements of the momentum operator can next be evaluated between states $|i\rangle \equiv |k, m\rangle$ and $|j\rangle \equiv |k', m'\rangle$. We now take for convenience the applied and local fields to lie in

a direction x normal to one of the box faces, such that the momentum operators along the x direction are

$$\langle i|\hat{p}_x|j\rangle = (-i\hbar)\frac{2\sqrt{2}}{a}\frac{mm'}{m^2-m'^2}[1-(-1)^{m+m'}]\delta_{k,k'}, \tag{11}$$

As $a \to \infty$, corresponding to a bulk free-electron metal, the matrix element vanishes, reflecting the fact that a free electron cannot conserve momentum and energy by absorbing a photon. For finite a the particle walls break the translational invariance of free space. The initial and final states in the electric dipole limit must differ in parity. The inter-sub-band coupling given in Eq. (11) leads to a electrical conductivity along the x direction which is given by

$$\frac{\sigma_x(\omega\to 0)}{\sigma_0} = \frac{(4n_c+1)(n_c-1)}{4n_c^2} - \frac{48}{\pi^2\Gamma^2 n_c^3}\mathrm{Re}\sum_{m=1}^{n_c} m^2(n_c^2-m^2)\times\begin{cases} -v\tan v, & \text{if } m \text{ is even} \\ v\cot v, & \text{if } m \text{ is odd}\end{cases} \tag{12}$$

where $\Gamma = \gamma/\varepsilon_0$ is the level broadening in units of the zero-point energy, $\varepsilon_0 = \hbar^2\pi^2/2m^*a^2$ is the zero-point energy of confinement in a cube of dimension a, $n_c = \mathrm{Int}[k_F a/\pi]$, $\sigma_0 = n_0 e^2\tau/m^*$ is the Drude conductivity, and $v = (\pi m/2)(1-i\Gamma/m^2)^{1/2}$. Equation (12) is obtained by first performing the integrals over k and k', which leaves a double summation over n and n'. The summation over n' is evaluated exactly [23] by exploiting the fact that the function $\cot(\pi x)$ has poles at $x = n$ for $n = 0, \pm 1, \pm 2, \ldots$. As the particle size grows, the electrical conductivity will be equal to the dc Drude conductivity; the small metallic cube ceases to be metallic as $n_c = 1$.

We are interested in the electrical conductivity for large a ($a \gg 0.18\,\mathrm{nm}$), or equivalently for $n_c \gg 1$, in which case the summation over n in the second term in Eq. (12) is approximated by an integral using the Euler–Maclaurin summation formula [26], which is given by

$$\Delta = 6\sqrt{2}\beta x\int_0^1 y^2(1-y^2)\left[\frac{\beta}{t}+2e^{-2\sqrt{2}/xt}\left(t\sin(xt)+\frac{\beta}{t}\cos(xt)\right)\right]dy \tag{13}$$

where $t = [y^2+(y^4+\beta^2)^{1/2}]^{1/2}$, $\beta = \hbar/\varepsilon_F\tau = 2/k_F l$, and $x = l/a$ with l the electron mean free path.

3. ELECTRONIC HEAT TRANSFER

For pure metals at room temperature, the mean free path between electrons (l_{e-e}) and the mean free path between electrons and defects (l_{e-d}) are much greater than the mean free path for electron–phonon interactions (l_{e-ph}). From elementary kinetic theory [27–28] and the equivalent thermal resistance schemes given in Ref. 8,

$$\frac{1}{\lambda_e} = \frac{1}{\lambda_{e-ph}} \tag{14}$$

In this equation, λ_e is the thermal conductivity associated with the conduction electrons in a material and λ_{e-ph} is the thermal conductivity due to electron–phonon interactions.

In general, λ_e is deduced from the electrical conductivity through the use of the Wiedemann–Franz law. The Wiedemann–Franz law is for materials in bulk form. However, some researchers [29–32] expect it is also suitable for micro- and nano-scale metallic materials. This is because it is only invalidated by inelastic electron scattering processes. Moreover, from a transport point of view, these metallic particles differ from the bulk materials primarily by the elastic electron and phonon scattering centers associated with disorders in the particle structure. Since the thermal conductivity of pure bulk samples is proportional to the electrical conductivity of the same samples via the Wiedemann–Franz law, the reduced thermal conductivity of small particles must also have the same proportionality with the reduced electrical conductivity of the same particles. Therefore,

$$\frac{\lambda_p}{\lambda_b} = \frac{\sigma_p}{\sigma_b}. \tag{15}$$

In small metallic particles, considering the influence of boundary scattering and the particle size, the average relaxation time is given by [33]

$$\frac{1}{\tau} = \frac{1}{\tau_b} + \frac{v}{R} \tag{16}$$

where τ_b is the electron relaxation time of the bulk crystal, v is the electron velocity equal to the Fermi velocity, and R is the particle radius. For pure nickel, τ_b is determined from the second order of the perturbation theory in pseudo-potential and the hybridization potential [34].

4. PHONON HEAT TRANSFER

To our knowledge, no experimentally measured phonon thermal conductivities for metals are available in the literature. Therefore, only

theoretical methods can be used to evaluate the thermal conductivity due to phonon heat transfer. For a pure metal, the influence of defects on the phonon heat transfer resistance is negligible because the mean free path between phonon–defect interactions (l_{ph-d}) is much higher than the phonon–phonon (l_{ph-ph}) and phonon–electron mean free paths (l_{ph-e}). From elementary kinetic theory [27, 28] and the equivalent thermal resistance schemes given in Ref. 8,

$$\frac{1}{\lambda_{ph}} = \frac{1}{\lambda_{ph-ph}} + \frac{1}{\lambda_{ph-e}} \tag{17}$$

Using elementary kinetic theory, we can get

$$\lambda_{ph-e} = \frac{l_{e-ph}}{l_{ph-ph}} \frac{n_{ph}}{n_e} \lambda_{ph-ph} \tag{18}$$

The electron velocity is taken equal to the Fermi velocity, $v_e = 2.04 \times 10^6 \mathrm{m \cdot s^{-1}}$, and the phonon velocity is equal to the sound velocity $v_{ph} = 5630 \mathrm{m \cdot s^{-1}}$ [35]. The volume specific heat and the phonon density are calculated from the Debye model [36].

The thermal conductivity due to phonon–phonon interactions in a thin nickel film is estimated using nonequilibrium molecular dynamics (NEMD) with the embedded-atom model (EAM). The two hard walls are maintained at $T_h = 350\,\mathrm{K}$ and $T_l = 250\,\mathrm{K}$; simulations are performed at constant density, with a film thickness range of 1.408–10.56 nm [37]. The theoretical thermal conductivity perpendicular to the film due to phonon-phonon interactions is obtained from the ballistic transport equation [38],

$$\lambda = 3nk_B \left(\frac{T}{\Theta_D}\right)^3 v^2 \int_0^{\Theta_D/T} \frac{x^4 e^x}{(e^x - 1)^2} \cdot \frac{1}{\frac{1}{\tau_b} + \frac{v}{dF}} dx \tag{19}$$

where n is the phonon density, v is the phonon velocity, Θ_D is the Debye temperature, τ_b is the bulk crystal phonon relaxation time, d is the film thickness, and F is the correction factor due to the influence of boundary scattering, which has the form [39],

$$\mathrm{F} = \frac{3}{4(2/\alpha - 1)} \tag{20}$$

where α is the phonon emissivity on the surface, $0 < \alpha < 1$, and $1 - \alpha$ denotes the energy loss due to elastic scattering and diffuse reflections on the surface.

For metallic particles, the thermal conductivity due to phonon–phonon interactions can be deduced from the corresponding film value calculated using the NEMD method. From Eqs. (16) and (19), assuming that the particle and the film have the same characteristic size and the same boundary scattering characteristics, the thermal conductivities of the films and particles are related as

$$\frac{\lambda_p}{\lambda_f} = \frac{\frac{1}{\tau_b} + \frac{v}{d\mathrm{F}}}{\frac{1}{\tau_b} + \frac{v}{R\mathrm{F}}} \tag{21}$$

where λ_p is the particle thermal conductivity due to phonon heat transfer, λ_f is the thermal conductivity perpendicular to the film due to phonon heat transfer, τ_b is the bulk crystal phonon relaxation time, v is the phonon velocity, R is the particle radius, d is the film thickness, and F is the correction factor defined in Eq. (20).

5. RESULTS AND DISCUSSION

Compared with other metals, nickel has a smaller electrical conductivity, so the electronic component of the thermal conductivity is also lower [8]. At room temperature ($T = 300\,\mathrm{K}$), the thermal conductivity of bulk nickel is $\lambda = 91.0\,\mathrm{W \cdot m^{-1} \cdot K^{-1}}$ [33]. The parameters in Table I were used to calculate the electronic contribution to the thermal conductivity of the particles. Equations (12), (15), and (16) are used to calculate the electrical conductivity in the nickel particles. The results in Fig. 2 show that the electrical conductivity increases as the particle size increases; however, it is less than the film value for the same characteristic size and boundary conditions. As the particle size grows, the electrical conductivity will be equal to the dc Drude conductivity, and as the particle size decreases to $\pi/k_F(n_c = 1)$, the particle will cease to be metallic.

Figure 3 shows that the thermal conductivity calculated from the electrical conductivity increases as the particle size increases; however, it is less than the thermal conductivity perpendicular to the film with the same characteristic size and boundary conditions. Thus, the particle size and

Table I. Basic Electron Parameters for Nickel at $T = 300\,\mathrm{K}$

$n(\mathrm{m^{-3}}s)$	18.26×10^{28}
$v(\mathrm{m \cdot s^{-1}})$	2.04×10^{6}
τ_b	3.76×10^{-15}

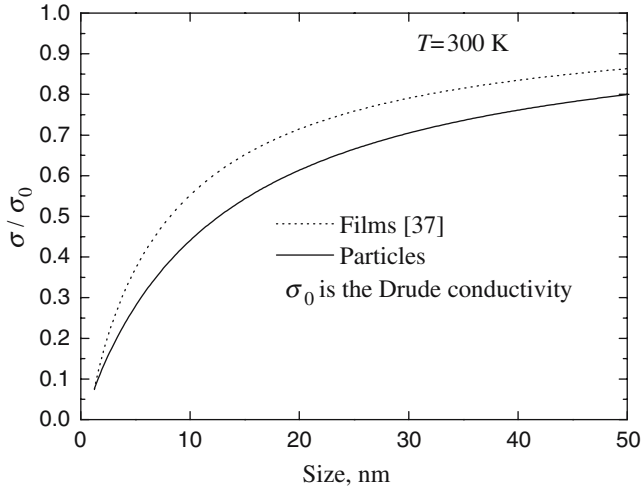

Fig. 2. Electrical conductivity variation for various particle sizes.

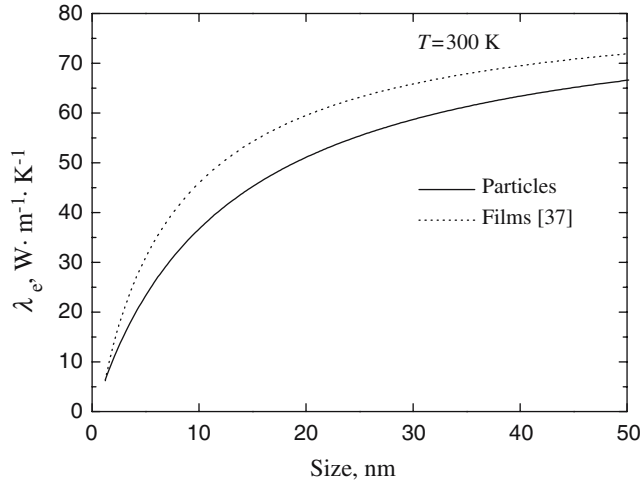

Fig. 3. Theoretical prediction of the electronic component of the thermal conductivity for various particle sizes.

boundary scattering are the main factors influencing the electronic component of the metallic particle thermal conductivity with the boundary scattering being much more dominant in the particles.

Figure 4 shows the variation of the thermal conductivity due to phonon heat transfer, phonon–phonon interactions, and phonon–electron

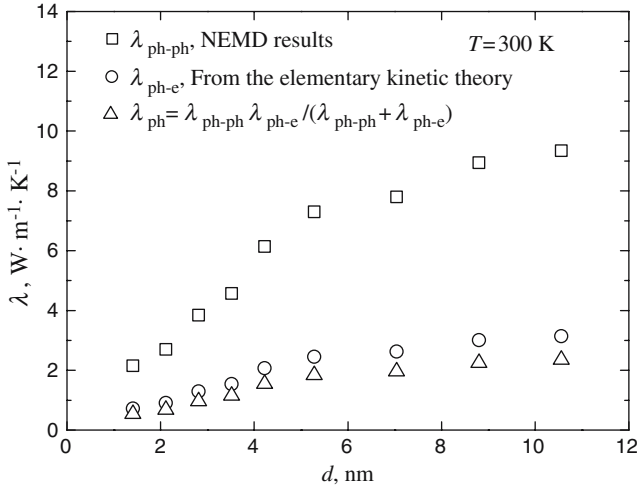

Fig. 4. Thermal conductivity due to phonon heat transfer and NEMD simulated results for various film thicknesses. The average temperature is 300 K, and the temperature gradient is 100 K.

interactions with the film thickness [37]. Figure 5 shows that the theoretical thermal conductivity perpendicular to the film due to phonon heat transfer given by Eq. (19) is close to the calculated results in Ref. 37 for $\alpha = 0.215$. Equation (19) can then be used to predict the thermal conductivity due to phonon heat transfer as a function of the film thickness. A relation between the bulk value of a parameter and the value obtained from an MD simulation proposed by Ercolessi [40] and the elementary kinetic theory is used to obtain the bulk thermal conductivity due to phonon heat transfer,

$$7.627\ \mathrm{W \cdot m^{-1} \cdot K^{-1}} < \lambda_{\mathrm{ph}}(b) < 7.700\ \mathrm{W \cdot m^{-1} \cdot K^{-1}}. \tag{22}$$

From the result in Eq. (22), the ratio of the thermal conductivity due to phonon heat transfer to the total thermal conductivity is about 8.5%. These results are realistic, as nickel is a good electrical conductor. The ratio would probably be less for other metals that have a larger electrical conductivity.

From Eq. (21) and the results in Fig. 4, the particle thermal conductivity due to phonon heat transfer can be calculated as shown in Fig. 6. Figure 6 shows that λ_{ph} increases with increasing particle size, and it is less than the thermal conductivity perpendicular to the film with the same characteristic size and boundary conditions. At $T = 300$ K, from phonon

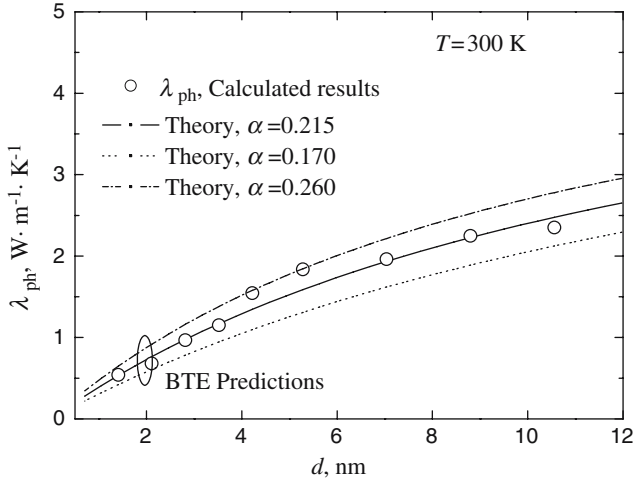

Fig. 5. Theoretical thermal conductivity perpendicular to the film due to phonon heat transfer and the calculated results for various film thicknesses [37].

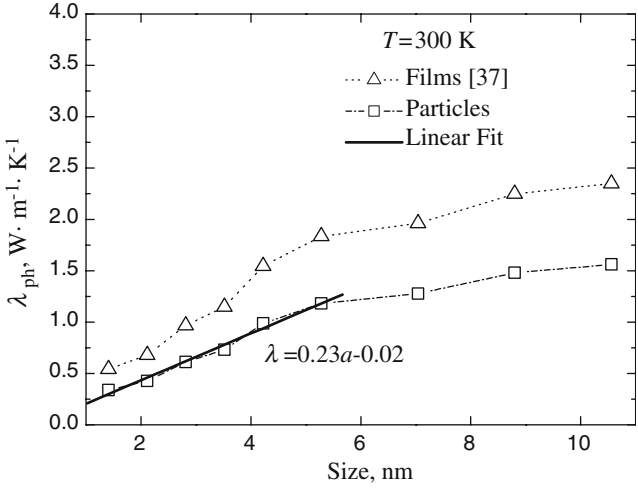

Fig. 6. Thermal conductivity due to phonon heat transfer for various particle sizes.

gas kinetic theory [41], a possible bulk nickel phonon mean free path (MFP) is estimated to be $l = 1.199 - 1.210$ nm; here $l - a$ is derived and the particle size can be taken as the effective phonon MFP in the small particles, and it gives the relation $\lambda \propto a$; and this is in good agreement

with calculated results for a particle size less than 6 nm as shown in Fig. 6. This analysis has attributed the conductivity size effect to that the particle size is the same order of magnitude as the phonon MFP in nanoscale small nickel particles.

From the results in Figs. 3 and 6, the thermal conductivity of small nickel particles can be calculated as shown in Fig. 7. Compared with the experimental value of the thermal conductivity of bulk nickel at $T = 300\,\mathrm{K}$, $91\,\mathrm{W \cdot m^{-1} \cdot K^{-1}}$, the 1.408 to 10.56 nm small particle thermal conductivity is about 2.5 to 10 times lower than that of bulk nickel, showing remarkable boundary scattering effects, quantum size effects, and size effects. Moreover, Fig. 7 shows that the total thermal conductivity of the particle is less than the total thermal conductivity perpendicular to the film with the same characteristic size due to the increased boundary scattering in the particle and that the difference between the film and particle total thermal conductivities decreases as the size increases. For very large and very small sizes, the total thermal conductivities of the films and the particles will be the same.

6. CONCLUSIONS

In metals, heat is mainly transferred by the diffusion of electrons, but experimental thermal conductivity curves suggest that, for metals with

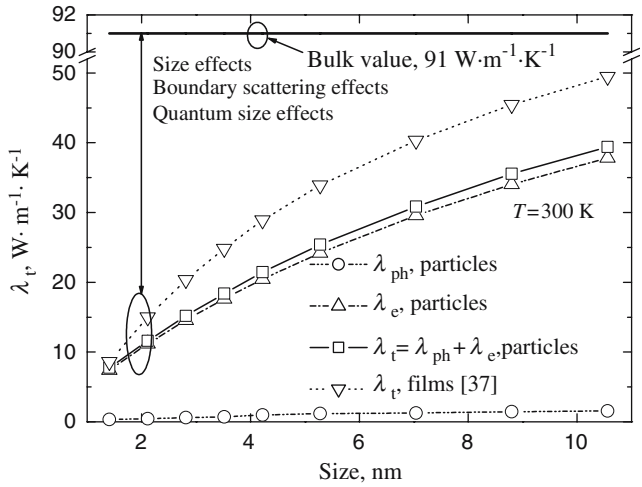

Fig. 7. Total thermal conductivity variation for various particle sizes.

lower electrical conductivities, the phonon heat transfer cannot be ignored [42]. In this paper, the thermal conductivity due to phonon heat transfer in small particles has been extrapolated from thin film results calculated using nonequilibrium molecular dynamics (NEMD) and the electronic contribution to the thermal conductivity of the particle has been deduced from the electrical conductivity through the use of the Wiedemann–Franz law. The electrical conductivity of small nickel particles has been estimated from the Kubo linear-response formalism with the relaxation time approximation. We find that the thermal conductivity of nanoscale small nickel particles has remarkable boundary scattering effects, quantum size effects, and size effects, which considers electrons only at the Fermi level and at a temperature lower than the Debye temperature. In a particle size range of 1.408–10.56 nm, the small particle thermal conductivity is about 2.5–10 times lower than that of bulk nickel at corresponding temperatures and decreases almost linearly as the particle size is reduced. The particle thermal conductivity is less than the film value for the same characteristic size and boundary conditions with a size range of 1–11 nm. The phonon size effect occurs because the effective phonon MFP is reduced when the particle is comparable to or even smaller than the phonon MFP in bulk nickel.

ACKNOWLEDGMENTS

This project was supported by the Specialized Research Fund for the Doctoral Program of Higher Education (No. 20020003004) and the National Outstanding Youth Fund from the National Natural Science Foundation of China (No. 50025617). We also thank Dr. David Christopher for editing the English.

REFERENCES

1. V. Bonacic-Koutecky, P. Fantucci, and J. Koutecky, *Chem. Rev.* **91**:1035 (1991).
2. V. A. Kurganov, Yu. A. Zeigarnik, I. V. Maslakova, F. P. Ivanov, and S. B. Martynov, *High Temp.* **38**:926 (2000).
3. I. M. L. Billas, J. A. Becker, A. Chatelain, and W. A. de Heer, *Science* **265**:1682 (1994).
4. S. E. Aspel, J. W. Emmert, J. Deng, and L. A. Bloomfield, *Phys. Rev. Lett.* **76**:1441 (1996).
5. Z. L. Wu, P. K. Kuo, L. H. Wei, S. L. Gu, and R. L. Thomas, *Thin Solid Films* **236**:191 (1993).
6. H. P. Myers, *Introductory Solid State Physics* (Taylor and Francis, London, 1990).
7. S. Kumar and G. C. Vradis, *J. Heat Transfer ASME* **116**:28 (1994).
8. P. Chantrenne, M. Raynaud, D. Baillis, and J. L. Barrat, *Microscale Thermophysical Eng.* **7**:117 (2003).
9. M. P. Allen and D. J. Tildesley, *Computer Simulation of Liquids* (Oxford University Press, New York, 1987).

10. D. Frenkel and S. Berend, *Understanding Molecular Simulation* (Academic Press, San Diego, 1996).
11. S. Papadia, B. Piveteau, and D. Spanjaard, *Phys. Rev. B* **54**:14720 (1996).
12. W. A. Harrison, *Pseudopotentials in the Theory of Metals* (Benjamin, New York, 1966).
13. Ş. Erkoç, B. Güneş, and P. Güneş, *Int. J. Mod. Phys. C* **11**:1013 (2000).
14. M. S. Daw and M. I. Baskes, *Phys. Rev. B* **29**:6443 (1984).
15. R. A. Johnson, *Phys. Rev. B* **37**:3924 (1988).
16. J. Mei, J. W. Davenport, and G. W. Fernando, *Phys. Rev. B* **43**:4653 (1991).
17. J. Cai and Y. Y. Ye, *Phys. Rev. B* **54**:8398 (1996).
18. S. S. Pohlong and P. N. Ram, *J. Mater. Res.***13**:1919 (1998).
19. B. Sadigh and G. Grimvall, *Phys. Rev. B* **54**:15742 (1996).
20. J. Z. Wang, M. Chen, and Z. Y. Guo, *Chin. Phys. Lett.* **19**:324 (2002).
21. H. E. Camblong and P. M. Levy, *Phys. Rev. B* **60**:15782 (1999).
22. C. Blass, P. Weinberger, L. Szunyogh, P. M. Levy, and C. B. Sommers, *Phys. Rev. B* **60**:492 (1999).
23. D. M. Wood and N. W. Ashcroft, *Phys. Rev. B* **25**:6255 (1982).
24. X. G. Zhang and W. H. Butler, *Phys. Rev. B* **51**:10085 (1995).
25. H. Bethe and E. Salpeter, *Quantum Mechanics of One- and Two-Electron Atoms* (Springer, Berlin, 1957).
26. C. M. Bender and S. A. Orzag, *Advanced Mathematical Methods for Scientists and Engineers* (McGraw-Hill, New York, 1978).
27. C. Kittel, *Introduction to Solid State Physics* (Wiley, New York, 1996).
28. N. W. Ashcroft and N. D. Mermin, *Solid State Physics* (Harcourt College Publishers, Fort Worth, Texas, 1976).
29. R. J. Anderson, *J. Appl. Phys.* **67**:6914 (1990).
30. C. L. Tien, B. F. Armaly, and P. S. Jagannathan, in *Thermal Conductivity* (Plenum Press, New York, 1969), pp. 13–19.
31. C. R. Tellier and A. J. Tosser, *Size Effects of Thin Films* (Elsevier, New York, 1982).
32. N. F. Mott and H. Jones, *Theory of Properties of Metals and Alloys* (Dover, New York, 1958).
33. U. Kreibig and C. V. Fragstein, *Z. Phys.* **224**:307 (1969).
34. V. T. Shvets, S. V. Savenko, and S. V. Datsko, *Condens. Matter Phys.* **7**:275 (2004).
35. E. T. Swartz and R. O. Pohl, *Rev. Modern Phys.* **61**:605 (1989).
36. S. P. Yuan and P. X. Jiang, in *Proc. 7th Asian Thermophys. Props. Conf.* (Hefei and Huangshan, Anhui, China, August 23–29, 2004).
37. S. P. Yuan and P. X. Jiang, *Prog. Natural Sci.* **15**:922 (2005).
38. A. Majumdar, *J. Heat Transfer ASME* **115**:7 (1993).
39. G. Chen and C. L. Tien, *AIAA J. Thermophys. Heat Transfer* **7**:311 (1993).
40. F. Ercolessi, *A Molecular Dynamics Primer* (International School for Advanced Studies (SISSA-ISAS), Trieste, Italy, Spring College in Computational Physics, ICTP, 1997).
41. J. M. Ziman, *Electrons and Phonons* (Oxford University Press, London, 1960).
42. Y. S. Touloukian, *Thermophysical Properties of Matter*, *Vol.1: Thermal Conductivity of Metallic Materials and Alloys* (Plenum Press, New York, 1970).